Title

Oxygen tension-mediated erythrocyte membrane interactions regulate cerebral capillary hyperemia.

Journal

Science advances, 5(5)

ISSN

2375-2548

Authors

Zhou, Sitong

Giannetto, Michael

DeCourcey, James

et al.

Publication Date

2019-05-01

DOI

10.1126/sciadv.aaw4466

BIOPHYSICS

Oxygen tension–mediated erythrocyte membrane interactions regulate cerebral capillary hyperemia

Sitong Zhou[1,2], Michael Giannetto[2], James DeCourcey[3], Hongyi Kang[2], Ning Kang[2], Yizeng Li[4], Suilan Zheng[5], Hetince Zhao[6], William R. Simmons[7], Helen S. Wei[8], David M. Bodine[7], Philip S. Low[5], Maiken Nedergaard[2]*, Jiandi Wan[2,9]*

The tight coupling between cerebral blood flow and neural activity is a key feature of normal brain function and forms the basis of functional hyperemia. The mechanisms coupling neural activity to vascular responses, however, remain elusive despite decades of research. Recent studies have shown that cerebral functional hyperemia begins in capillaries, and red blood cells (RBCs) act as autonomous regulators of brain capillary perfusion. RBCs then respond to local changes of oxygen tension (PO_2) and regulate their capillary velocity. Using ex vivo microfluidics and in vivo two-photon microscopy, we examined RBC capillary velocity as a function of PO_2 and showed that deoxygenated hemoglobin and band 3 interactions on RBC membrane are the molecular switch that responds to local PO_2 changes and controls RBC capillary velocity. Capillary hyperemia can be controlled by manipulating RBC properties independent of the neurovascular unit, providing an effective strategy to treat or prevent impaired functional hyperemia.

INTRODUCTION

Thinking, reading, writing, and throwing a baseball are all activities in which neural activity is coupled with local elevation in cerebral blood flow. This coupling is a hallmark of normal brain function and forms the basis of functional hyperemia (*1*, *2*). Functional hyperemia plays critical roles in functional brain imaging (*3*, *4*), and defects in functional hyperemia are believed to contribute to synaptic loss and cognitive decline in multiple neurodegenerative diseases including Alzheimer's disease (*5*–*8*). The question of what drives functional hyperemia, however, is still unclear despite decades of research (*1*, *9*–*13*). Most recently, it has emerged that cerebral functional hyperemia is initiated in capillaries rather than upstream in arterioles in the brain, thus challenging the existing dogma that the capillary bed is a passive conduit for upstream vasodilation (*14*, *15*). Several initial publications have suggested that pericytes control capillary blood flow, but later studies could not confirm contractility of pericytes (*16*–*19*). In particular, the third-order branches of capillary pericytes do not express smooth muscle actin and should therefore be unable to constrict (*15*, *16*). Our group has shown recently that the initial (transient) dip in tissue oxygen tension (PO_2) after hindlimb stimulation drives brain capillary hyperemia, and furthermore, that PO_2 can itself, independent of the neurovascular unit, control red blood cell (RBC) deformability, thus modulating RBC flow through capillaries (*15*). Hence, RBCs are active players in capillary hyperemia and promptly increase O_2 delivery in response to activity-induced local changes in PO_2. RBC-mediated capillary hyperemia provides a simple yet robust mechanism for swift and precise local increases in capillary flow in response to the ever-changing patterns of neural activity within the central nervous system. However, the underlying mechanisms of how RBCs control their deformability and capillary velocity in response to changes of local PO_2 remain elusive.

We hypothesize that deoxygenated hemoglobin (deoxyHb) and band 3 interactions on RBC membrane disrupt the band 3–ankyrin linkage during RBC deoxygenation (Fig. 1A), resulting in membrane detachment and increased RBC deformability and, consequently, an elevated capillary velocity. PO_2 has been shown to be able to regulate multiple RBC activities including glucose metabolism (*20*, *21*), cation transport (*22*), adenosine triphosphate release (*23*, *24*), and cytoskeletal organization (*24*–*27*). The reversible binding of deoxyHb with band 3, in particular, has been postulated to be critical in many of these processes. This is because the cytoplasmic domain of band 3 contains the only known Hb binding site on the RBC membrane and Hb–band 3 interactions are strongly O_2 dependent (*28*–*30*). Here, to address the hypothesized roles of Hb–band 3 interactions in PO_2-mediated capillary hyperemia, we combined ex vivo microfluidics and in vivo two-photon microscopy and meticulously examined RBC deformability and capillary velocity as a function of PO_2 using RBCs from human, wild-type (WT) mice, and transgenic mice that have modified RBC deoxyHb–band 3 interactions. Moreover, the dynamics of PO_2-mediated RBC capillary velocity and the quantitative relation between RBC deformability and capillary velocity were unveiled to shed light on the governing physical principles of capillary hyperemia. Last, we would like to emphasize that because RBCs circulate in the circulatory system throughout the entire body, the demonstrated roles of PO_2 in the regulation of RBC capillary velocity are not only limited to the brain but also apply to any organs with high oxygen consumption.

[1]Microsystems Engineering, Rochester Institute of Technology, Rochester, NY 14623, USA. [2]Center for Translational Neuromedicine, University of Rochester Medical Center, Rochester, NY 14642, USA. [3]College of Osteopathic Medicine, University of New England, Biddeford, ME 04005, USA. [4]Department of Mechanical Engineering, Johns Hopkins University, Baltimore, MD 21218, USA. [5]Department of Chemistry, Purdue University, West Lafayette, IN 47907, USA. [6]New York University Langone Medical Center, New York, NY 10010, USA. [7]National Human Genome Research Institute, Bethesda, MD 20894, USA. [8]Rutgers New Jersey Medical School, Newark, NJ 07101, USA. [9]Department of Chemical Engineering, University of California, Davis, Davis, CA 95616, USA.
*Corresponding author. Email: maiken_nedergaard@urmc.rochester.edu (M.N.); jdwan@ucdavis.edu (J.W.)

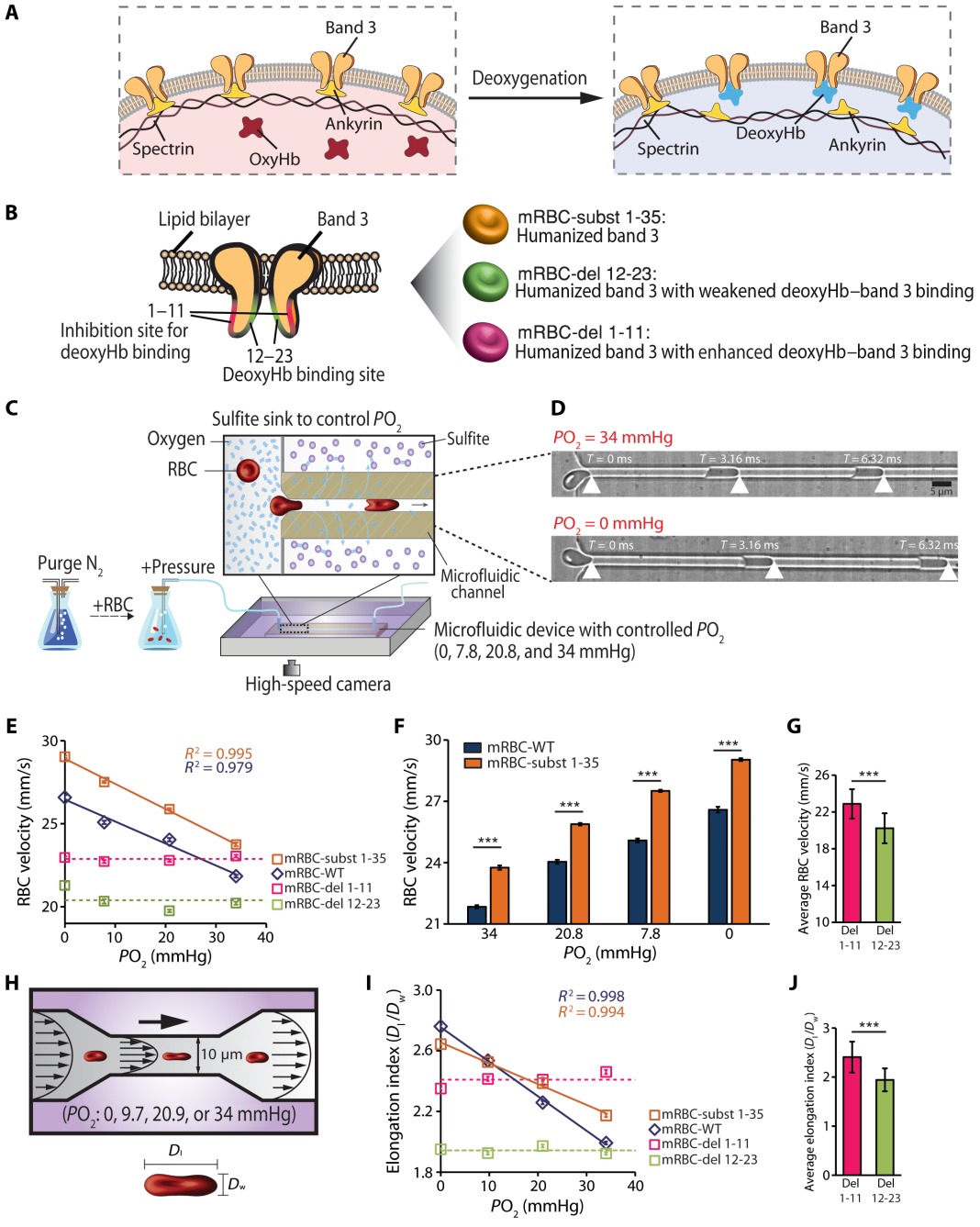

Fig. 1. DeoxyHb–band 3 interactions regulate PO_2-mediated RBC capillary velocity. (**A**) Schematics of the hypothesized Hb–band 3 interactions during deoxygenation. The binding of deoxyHb to band 3 during RBC deoxygenation weakens the band 3–ankyrin interactions, resulting in more deformable RBCs. (**B**) Schematics of transgenic mouse RBCs (mRBCs) with modified deoxyHb–band 3 interactions. (**C**) Microfluidic setup for ex vivo analysis of PO_2-mediated RBC velocity in capillary. The microfluidic device was submerged in a sulfite sink with 0, 0.01, 0.1, or 1 M sodium sulfite to control the PO_2 inside the microfluidic channel. A high-speed camera was used to record RBC motion in the capillary. (**D**) Time-lapse images showed that mRBCs flow faster at reduced PO_2. Scale bar, 5 μm. (**E**) mRBC velocity in capillary as a function of PO_2. The velocity of mRBC-WT and mRBC-subst 1-35 changes linearly with PO_2 [mRBC-WT: $n = 146$, RBC velocity (mm/s) = $-0.132 \times PO_2$ (mmHg) + 26.455, $R^2 = 0.979$; mRBC-subst 1-35: $n = 149$, RBC velocity (mm/s) = $-0.151 \times PO_2$ (mmHg) + 28.913, $R^2 = 0.995$]. (**F**) The velocity of mRBC-WT is significantly lower than that of mRBC-subst 1-35 at each PO_2 level. ***$P < 0.001$, t test. (**G**) The velocity of mRBC-del 1-11 and mRBC-del 12-23 is not sensitive to surrounding PO_2 changes and remains relatively constant at 22.88 ± 1.59 mm/s ($n = 157$) and 20.23 ± 1.63 mm/s ($n = 115$), respectively. ***$P < 0.001$, t test. (**H**) A schematic of the experimental setup for ex vivo analysis of RBC deformability as a function of PO_2. The deformability of RBCs was characterized by the elongation index D_l/D_w, where D_l and D_w were, respectively, the length and thickness of an RBC flowing through the constriction. (**I**) The elongation index (D_l/D_w) of mRBC-WT and mRBC-subst 1-35 increased linearly as the decrease of PO_2 [mRBC-WT: $n = 209$, $D_l/D_w = -0.0228 \times PO_2$ (mmHg) + 2.7548, $R^2 = 0.998$; mRBC-subst 1-35: $n = 195$, $D_l/D_w = -0.0137 \times PO_2$ (mmHg) + 2.6545, $R^2 = 0.994$]. (**J**) The elongation index of mRBC-del 1-11 and mRBC-del 12-23 was not sensitive to PO_2 changes and remains relatively constant at 2.41 ± 0.31 ($n = 195$) and 1.94 ± 0.23 ($n = 194$), respectively. ***$P < 0.001$, t test. Error bars are shown as SE.

RESULTS

DeoxyHb–band 3 interactions regulates PO_2-mediated RBC capillary velocity

To explore the roles of deoxyHb–band 3 interactions in PO_2-mediated RBC capillary velocity, we examined ex vivo RBC velocity in a microfluidic capillary using RBCs from three transgenic mice that had modified deoxyHb–band 3 interactions (Fig. 1B) (*24*). The first strain of mouse had RBCs where the NH_2-terminal residues 1 to 45 on the cytoplasmic domain of band 3 were replaced by the homologous sequence (residues 1 to 35) of human band 3 [transgenic mouse RBC (mRBC)–subst 1-35] (*27*). mRBC-subst 1-35 thus had the "humanized" band 3 and was used together with RBCs from WT mice (mRBC-WT) as control. RBCs from the second strain of mouse had the same humanized band 3 except that the deoxyHb–band 3 binding site, residues 12 to 23, was deleted (mRBC-del 12-23). As a result, deoxyHb–band 3 interactions in mRBC-del 12-23 were substantially weakened. RBCs from the third strain also had the same humanized band 3, but a homologous sequence (1-MEELQDDYEDM-11) adjacent to residues 12 to 23 of band 3 was removed (mRBC-del 1-11). Because residues 1 to 11 are known to inhibit band 3 interactions with deoxyHb, removal of residues 1 to 11 enchances deoxyHb–band 3 interactions (*27*). We used RBCs from these three strains of mouse together with mRBC-WT to examine RBC velocity as a function of PO_2 in microfluidics (Fig. 1C). In particular, we dispersed RBCs into a phosphate-buffered saline (PBS) buffer that was purged by N_2 overnight. We then injected the RBC suspension at a constant pressure (1.1×10^4 Pa) into a polydimethylsiloxane (PDMS) microfluidic device containing a constriction capillary ($w_c = 3$ μm; $h = 4.5$ μm). We immersed the entire microfluidic device in an aqueous sink containing sodium sulfite (an O_2 scavenger) and controlled the PO_2 inside the microfluidic channel by varying the sulfite concentration (fig. S1A). We recorded the motion of RBCs as a function of PO_2 in the constriction using a high-speed camera (Fig. 1D). Consistent with previous findings in human RBCs (hRBCs) (*15*), the velocity of mRBC-WT and mRBC-subst 1-35 increased linearly with the decrease in PO_2 (Fig. 1E). The sensitivity of RBC velocity to PO_2 changes (slope of the fitting curve) was not significantly different between mRBC-WT and mRBC-subst 1-35 (fig. S1B). The velocity of mRBC-subst 1-35, however, was significantly higher than that of mRBC-WT at each PO_2 level (Fig. 1F). Notably, when RBCs with enhanced (mRBC-del 1-11) or weakened (mRBC-del 12-23) deoxyHb–band 3 interactions were used, we completely abolished the dependence of RBC velocity on PO_2 (Fig. 1E). In addition, the average velocity of mRBC-del 12-23 was significantly lower than that of mRBC-del 1-11 (Fig. 1G). These results demonstrate that modification of deoxyHb–band 3 interactions affects the sensitivity of RBC velocity to PO_2 changes and reduced band 3–deoxyHb interactions lead to decreased RBC capillary velocity.

Because rheological properties of RBCs relate tightly to RBC velocity in microvessels, we next examined whether deoxyHb–band 3 interactions also regulated RBC deformability. Figure 1H showed the microfluidic setup where a relatively wide constriction ($w_c = 10$ μm; $h = 7.4$ μm) was used to measure shear-induced elongation of RBCs. PO_2 in the constriction was controlled by the sulfite sink (fig. S1C). We characterized the shear-induced RBC elongation using the elongation index, D_l/D_w, where D_l and D_w were, respectively, the length and thickness of an RBC flowing through the constriction. As shown in Fig. 1I, elongation index of mRBC-WT and mRBC-subst 1-35 increased linearly with the decrease in PO_2, indicating increased RBC deformability at reduced PO_2. When RBCs with modified deoxyHb–band 3 interactions were used (mRBC-del 12-23 and mRBC-del 1-11), the elongation index of these RBCs was not dependent on PO_2, and the average elongation index of mRBC-del 12-23 was significantly smaller than that of mRBC-del 1-11 (Fig. 1J). These sets of data show that deoxyHb–band 3 interactions regulate RBC deformability during RBC deoxygenation and that the change of RBC deformability correlates tightly with RBC capillary velocity.

Transgenic mice with modified deoxyHb–band 3 interactions exhibit PO_2-independent capillary hyperemia in vivo

Although ex vivo microfluidic experiments demonstrated that the dependence of RBC capillary velocity on PO_2 could be manipulated by altering the RBC deoxyHb–band 3 interactions, whether RBC deoxyHb–band 3 interactions affect in vivo capillary hyperemia remained unknown. To address this question, we used a laser scanning two-photon microscope to measure in vivo RBC capillary velocity as a function of tissue PO_2 in the cerebral cortex of WT mice (mRBC-WT) and transgenic mice (mRBC-subst 1-35, mRBC-del 1-11, and mRBC-del 12-23). Under the guidance of two-photon imaging, we microinjected sodium sulfite solution to the hindlimb cortex of a mouse brain to control local tissue PO_2 near capillaries (Fig. 2A). Microinjection of sulfite triggered a rapid decrease in local tissue PO_2, and these PO_2 dips increased as the sulfite concentration was elevated (Fig. 2B). Note that the biphasic pattern of PO_2 response to sulfite injection, e.g., an initial transient dip followed by a delayed long-lasting overshoot, was similar to previously observed activity-dependent PO_2 responses (*15*). We then measured RBC velocity in capillaries as a function of local tissue PO_2 using two-photon line scan. A typical line-scan image acquired with longitudinal line scan before and after sulfite injection in mRBC-WT is shown in Fig. 2C, where x represents the scanning distance and t is time. Each RBC in the line-scan image appeared as a black stripe, and the slope of the stripe represented RBC velocity, v, which increased upon sulfite injection. In mRBC-WT and mRBC-subst 1-35 mice, the peak velocity and the increase of peak velocity relative to the baseline velocity upon 1 M sulfite injection were significantly higher than that upon 0.01 M sulfite injection (Fig. 2, D and E, and fig. S2), suggesting that in vivo RBC capillary velocity was regulated by local PO_2 changes in control mice. In contrast, the peak velocity and the increase of peak velocity after sulfite injection in mRBC-del 1-11 mice (Fig. 2F) and mRBC-del 12-33 mice (Fig. 2G) did not change with the increase in sulfite, suggesting that local PO_2 changes failed to regulate RBC capillary velocity when RBC deoxyHb–band 3 interactions were modified. Note that although the increase of capillary velocity did not change with sulfite concentration, capillary velocity did increase upon sulfite injection in mRBC-del 1-11 and mRBC-del 12-33 mice. This is likely due to the increase of blood flow upstream in arterioles after sulfite injection (*15*), supported by the observed long onset time of capillary velocity increase in mRBC-del 12-33 (Fig. 2H). These results are consistent with our ex vivo findings and show that in vivo capillary hyperemia is controlled by RBC deoxyHb–band 3 interactions.

Biochemical modulation of deoxyHb–band 3 interactions in WT RBCs regulates PO_2-mediated RBC capillary velocity

To further evaluate the roles of deoxyHb–band 3 interactions in PO_2-mediated RBC capillary velocity, we varied deoxyHb–band 3

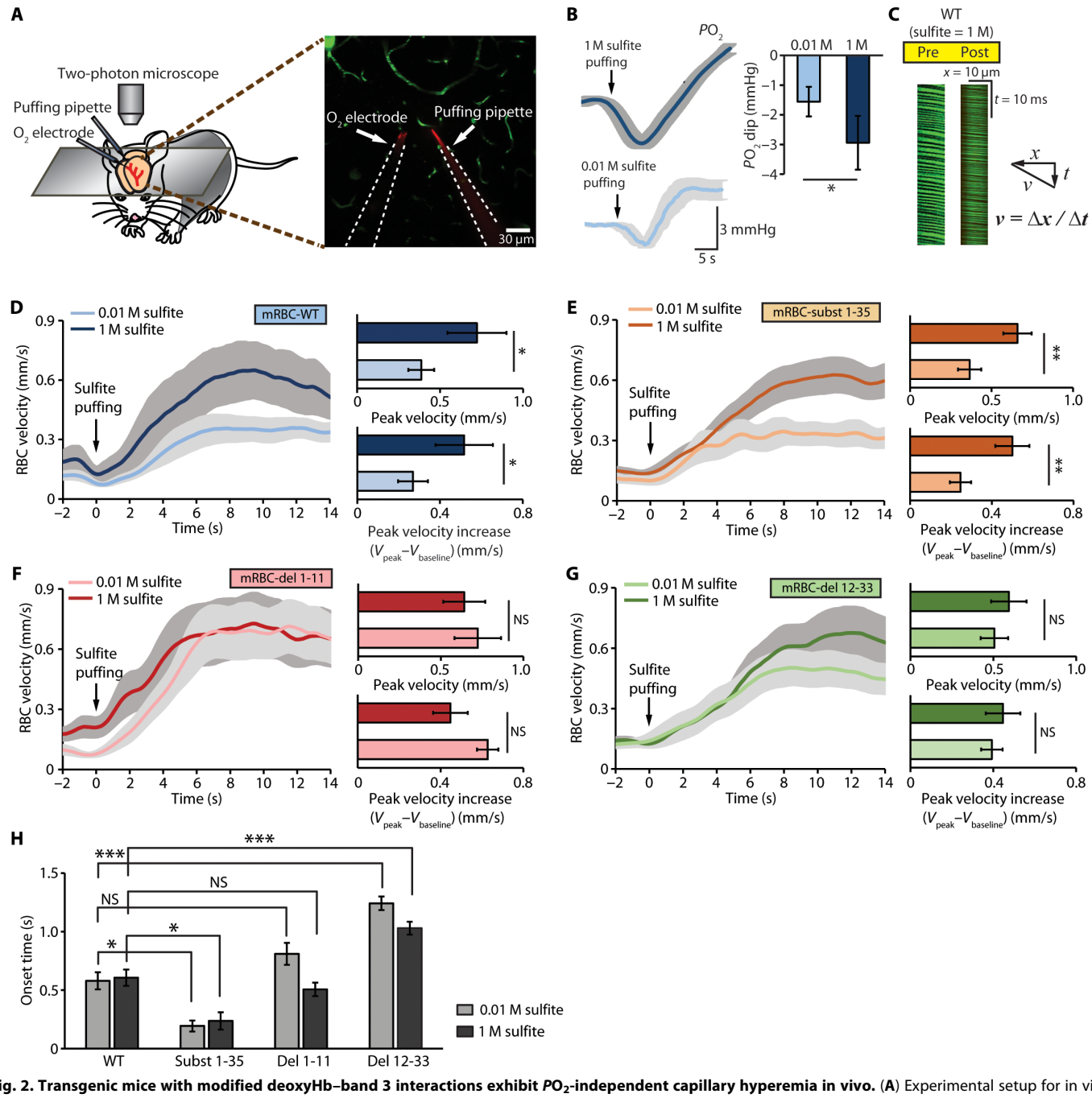

Fig. 2. Transgenic mice with modified deoxyHb–band 3 interactions exhibit PO_2-independent capillary hyperemia in vivo. (**A**) Experimental setup for in vivo assessing cerebral capillary hyperemia and tissue PO_2 upon locally applied O_2 scavenger (sodium sulfite, 0.01 and 1 M) in a mouse cerebral cortex. Through a cranial window, sodium sulfite was microinjected by a micropipette inserted 100 to 150 μm below the pial surface and placed <50 μm from a capillary. Puffing micropipette and O_2 sensor microelectrode were placed in close proximity (<50 μm). RBC velocity in capillary was imaged using two-photon laser scanning microscopy. Scale bar, 30 μm. (**B**) Local changes of PO_2 were dose dependent on the concentration of microinjected sulfite. The transient reduction in PO_2 was followed by a PO_2 overshoot. $n = 12$ and 4 mice. *$P < 0.05$, t test. (**C**) Typical images of the two-photon line scan of a capillary before and after the microinjection of sulfite. Black stripes represented RBCs. RBC velocity was obtained by calculating the slopes of the stripes. (**D**) Time-course plot of RBC capillary velocity increases after microinjection of sulfite for WT mice (mRBC-WT; $n = 217$ capillaries and 10 mice) and transgenic mice with (**E**) humanized band 3 (mRBC-subst 1-35; $n = 153$ capillaries and 8 mice), (**F**) enhanced deoxyHb–band 3 interactions (mRBC-del 1-11; $n = 243$ capillaries and 10 mice), and (**G**) weakened deoxyHb–band 3 interactions (mRBC-del 12-23; $n = 243$ capillaries and 10 mice). *$P < 0.05$, **$P < 0.01$, t test. (**H**) The onset time of increase of RBC capillary velocity after sulfite puffing in WT and transgenic mice. *$P < 0.05$, ***$P < 0.001$, t test. Error bars are shown as SE. NS, not significant.

and band 3–cytoskeletal interactions in mRBC-WT and hRBCs via phosphoenolpyruvate (PEP), sodium phosphate (Pi), or pervanadate treatment (Fig. 3A) (*28*, *31*–*33*). PEP treatment increased intracellular concentration of 2,3-diphosphoglyceric acid (2,3-DPG) in RBCs, whereas Pi treatment decreased 2,3-DPG concentration (fig. S3A). Because 2,3-DPG binds preferably to deoxyHb (*34*), increase or decrease of 2,3-DPG will change the amount of deoxyHb available to band 3. This change of deoxyHb is thus expected to alter the magnitude and kinetics of deoxyHb–band 3 interactions (*28*) and consequently affects PO_2-mediated RBC capillary velocity. The sensitivity of RBC velocity to PO_2 changes (slope of the fitting curve) was significantly reduced when RBCs were treated with PEP and Pi (Fig. 3, B and C, and fig. S3B). At each PO_2 level, the velocity of RBCs treated with PEP was significantly lower than

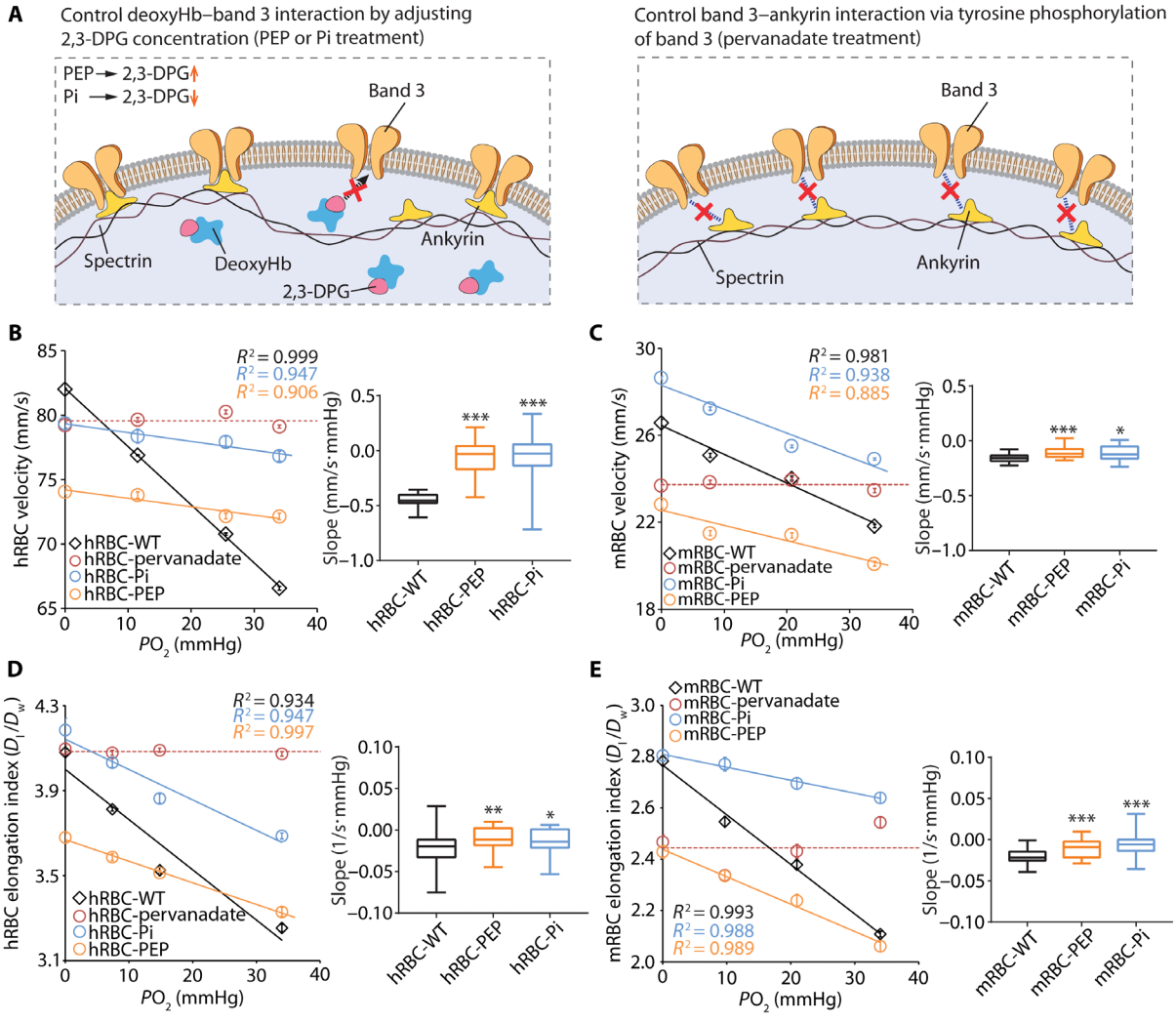

Fig. 3. Biochemical modulation of deoxyHb–band 3 interactions regulates PO_2-mediated RBC capillary velocity. (**A**) Left: DeoxyHb–band 3 interactions are manipulated by increasing (via PEP treatment) or decreasing (via Pi treatment) intracellular concentration of 2,3-DPG. Right: Tyrosine phosphorylation of band 3 (via pervanadate treatment) promotes dissociation of band 3 from the spectrin-actin skeleton. (**B**) The velocity of hRBC-WT, hRBC-Pi, and hRBC-PEP decreased linearly with the increase of PO_2 [hRBC-WT: $n = 71$, RBC velocity (mm/s) = $-0.451 \times PO_2$ (mmHg) + 82.074, $R^2 = 0.999$; hRBC-Pi: $n = 174$, RBC velocity (mm/s) = $-0.068 \times PO_2$ (mmHg) + 79.332, $R^2 = 0.947$; hRBC-PEP: $n = 167$, RBC velocity (mm/s) = $-0.065 \times PO_2$ (mmHg) + 74.198, $R^2 = 0.906$]. The velocity of hRBC-pervanadate was not sensitive to PO_2 changes and remained constant at 79.56 ± 0.28 mm/s ($n = 198$). Compared to hRBC-WT, the sensitivity of RBC velocity to PO_2 changes (as indicated by the slope) was reduced in hRBC-Pi and hRBC-PEP. ***$P < 0.001$, *t* test. (**C**) The velocity of mRBC-WT, mRBC-Pi, and mRBC-PEP decreased linearly with the increase of PO_2 [mRBC-WT: $n = 146$, RBC velocity (mm/s) = $-0.132 \times PO_2$ (mmHg) + 26.455, $R^2 = 0.981$; mRBC-Pi: $n = 159$, RBC velocity (mm/s) = $-0.11 \times PO_2$ (mmHg) + 28.296, $R^2 = 0.938$; mRBC-PEP: $n = 146$, RBC velocity (mm/s) = $-0.071 \times PO_2$ (mmHg) + 22.557, $R^2 = 0.885$]. Compared to mRBC-WT, the sensitivity of RBC capillary velocity to PO_2 changes was reduced after Pi and PEP treatments. *$P < 0.05$, ***$P < 0.001$, *t* test. (**D**) The elongation index of hRBC-WT, hRBC-Pi, and hRBC-PEP decreased linearly with the increase of PO_2 [hRBC-WT: $n = 239$, $D_l/D_w = -0.0236 \times PO_2$ (mmHg) + 4.0001, $R^2 = 0.934$; hRBC-Pi: $n = 132$, $D_l/D_w = -0.0143 \times PO_2$ (mmHg) + 4.142, $R^2 = 0.947$; hRBC-PEP: $n = 144$, $D_l/D_w = -0.0102 \times PO_2$ (mmHg) + 3.6698, $R^2 = 0.997$]. hRBC-pervanadate deformation was not sensitive to PO_2 changes and remained constant at 4.08 ± 0.02 mm/s ($n = 216$). *$P < 0.05$, **$P < 0.01$, *t* test. (**E**) The elongation index of mRBC-WT, mRBC-Pi, and mRBC-PEP decreased linearly with the increase of PO_2 [mRBC-WT: $n = 207$, $D_l/D_w = -0.0228 \times PO_2$ (mmHg) + 2.7548, $R^2 = 0.993$; mRBC-Pi: $n = 125$, $D_l/D_w = -0.005 \times PO_2$ (mmHg) + 2.8088, $R^2 = 0.988$; mRBC-PEP: $n = 120$, $D_l/D_w = -0.0107 \times PO_2$ (mmHg) + 2.4383, $R^2 = 0.989$]. mRBC-pervanadate deformation was not sensitive to PO_2 changes and remained relatively constant at 2.44 ± 0.03 mm/s ($n = 216$). ***$P < 0.001$, *t* test. Error bars are shown as SE.

that of RBCs treated with Pi (fig. S3, C and D). In addition, when RBCs were treated with pervanadate that directly triggered tyrosine phosphorylation of band 3 and induced the dissociation of band 3 from its ankyrin linkage to the spectrin-actin skeleton (*32*), the dependence of RBC velocity on PO_2 was completely abolished (Fig. 3, B and C). The velocity of RBCs treated with pervanadate was also significantly higher than that of RBCs treated with PEP at different PO_2 levels (fig. S3, C and D). These observations demonstrate that intracellular 2,3-DPG concentration and band 3 phosphorylation regulate PO_2-mediated RBC capillary velocity in WT RBCs, likely via the modulation of deoxyHb–band 3 and band 3–cytoskeletal interactions, respectively. In addition, the sensitivity of RBC deformation to PO_2 changes was significantly reduced after PEP and Pi treatments and diminished after pervanadate treatment (Fig. 3, D and E, and fig. S3E). The magnitude of elongation index at each PO_2 level was lower for RBCs treated with PEP compared to RBCs treated with Pi and pervanadate (fig. S3, F and G). These results show that 2,3-DPG concentration and band 3 phosphorylation control RBC deformation. Moreover, the similar trend between RBC deformation and capillary velocity as a function of PO_2 after PEP, Pi, and pervanadate treatments highlights again the tight correlation between RBC deformability and its capillary velocity.

Dynamics of PO_2-mediated RBC capillary velocity

Although the results from both ex vivo and in vivo experiments have shown that deoxyHb–band 3 and band 3–cytoskeletal interactions contribute to PO_2-mediated RBC capillary velocity, several critical questions still remain. For example, if the band 3–ankyrin linkage is ruptured during RBC deoxygenation, then the RBC membrane will be released from its underlying cytoskeletal network. If so, is there any evidence showing RBC membrane detachment during deoxygenation? Does the duration of deoxygenation play a role in such a process and in PO_2-mediated RBC capillary velocity? How can one quantitatively relate RBC capillary velocity to its deformability?

To answer these questions, we first examined the change of RBC membrane-cytoskeletal interactions during deoxygenation by measuring RBC tank-treading frequency as a function of PO_2. Tank-treading motion of an RBC refers to the rotation of the RBC membrane around the cell body, which usually occurs in a shear flow. The velocity of this motion is mainly determined by the applied shear rate, viscosity of the suspending medium, and the membrane-cytoskeletal interactions. Thus, RBCs with disrupted membrane-cytoskeletal interactions are expected to have an increased tank-treading velocity, given that the shear rate and medium viscosity are constant. Figure 4A shows the microfluidic setup where a microfluidic channel with a constriction (w_c = 20 μm; h = 38 μm) was used to induce RBC tank-treading motion in flow. hRBCs attached with microspheres (1 μm, polystyrene) were injected to the microfluidic channel, and the tank-treading frequency [f (s^{-1})], which is the inverse of the orbital period (the time for the microbead moving along with the RBC) membrane to complete one revolution), was measured using a high-speed camera. In addition, we varied the length of the channel before constriction (600, 4200, and 12,000 μm) to examine whether the exposure time of reduced PO_2, t_{total}, affected RBC tank-treading motion. In these sets of experiments, t_{total} was controlled at 18 ± 4, 192 ± 30, and 377 ± 11 ms. We calibrated PO_2 inside the channel as described previously (fig. S4A). The results showed that the normalized tank-treading frequency, f (s^{-1})/f $(s^{-1})_{34mmHg}$, where f $(s^{-1})_{34mmHg}$, is the tank-treading frequency measured at PO_2 = 34 mmHg, increased linearly with the decrease in PO_2 when t_{total} was 192 ± 30 and 377 ± 11 ms and was independent of PO_2 changes when t_{total} was 18 ± 4 ms (Fig. 4B). The sensitivity of the tank-treading frequency to PO_2 changes was also increased with the increase in t_{total} and medium viscosity (Fig. 4C and fig. S4B). RBC tank-treading frequency increased with the increase in viscosity of the RBC suspension (*35*), particularly at low PO_2 levels (fig. S4C). Collectively, the facts that RBC tank-treading frequency increased at reduced PO_2 and the sensitivity of tank-treading frequency to PO_2 increased with t_{total} support evidently that RBC membrane is detached during deoxygenation and the duration of reduced PO_2 plays a regulatory role.

The observed effect of t_{total} on RBC tank-treading frequency led us to hypothesize that t_{total} might also regulate RBC capillary velocity. To test the hypothesis, we measured RBC velocity in a series of microfluidic capillaries under controlled t_{total} (fig. S4D). The results shown in Fig. 4D demonstrated that the normalized RBC velocity, V_{0mmHg}/V_{34mmHg}, where V_{0mmHg} and V_{34mmHg} were the RBC velocity at PO_2 = 0 mmHg and 34 mmHg, respectively, was independent of t_{total} for transgenic mice with modified band 3–deoxyHb interactions (mRBC-del 1-11 and mRBC-del 12-23). In contrast, the normalized RBC velocity of hRBC-WT, mRBC-subst 1-35, and mRBC-WT increased with the increase in t_{total} and reached a maximum velocity at a threshold t_{total} of 462 ± 71, 913.4 ± 63, and 955.1 ± 57 ms, respectively. Notably, the critical t_{total} of mRBC-subst 1-35 is shorter than that of mRBC-WT, consistent with the shortest onset time in mRBC-subst 1-35 observed in vivo (Fig. 2H). These results thus show that the duration of reduced PO_2 regulates RBC capillary velocity and that there is a critical PO_2 exposure time beyond which RBC capillary velocity reaches a plateau and does not change with further increase in PO_2 exposure time.

Last, we evaluate the correlation between RBC capillary velocity and RBC deformability by analyzing the changes of RBC width r_0 in capillary as a function of PO_2 (Fig. 4E). As shown in Fig. 4F, the normalized cell width, $r_0/r_{0\ 34mmHg}$, where $r_{0\ 34mmHg}$ is the cell width measured at PO_2 = 34 mmHg, decreased with the decrease in PO_2, whereas RBC capillary velocity increased concurrently, implying that RBC capillary velocity increases as r_0 decreases. According to the classical Bretherton scaling for a long bubble flowing in a microchannel, the surface tension of the gas bubble σ relates to its radius in channel $r_{0\ bubble}$ by $Ca^{2/3} = (\mu v/\sigma)^{2/3} \propto (R_0 - r_{0\ bubble})/R_0$, where R_0 is the radius of the microchannel, $Ca = \mu v/\sigma$ is the capillary number, μ is the viscosity, and v is the velocity. Applying the Bretherton scaling to RBCs flowing in a capillary and replacing $r_{0\ bubble}$ and σ with RBC width r_0 and RBC membrane tension E (assuming E is uniform on RBC), respectively, we obtain $(\mu v/E)^{2/3} \propto (R_0 - r_0)/R_0$. A small E, e.g., a more deformable RBC, thus corresponds to a large gap distance ($R_0 - r_0$) and, consequently, a small r_0, given that R_0 is constant. As a result, RBCs with increased deformability will have a small r_0 when flowing in a capillary, and a small r_0 correlates to a high RBC capillary velocity, as experimentally observed in Fig. 4F. To further quantitatively assess the relation between r_0 and RBC capillary velocity, we calculated the shear stress acting on RBCs in capillary using lubrication approximation and showed that the nondimensional RBC capillary velocity is a function of r_0 (fig. S4E). Therefore, RBC capillary velocity relates to RBC deformability through the change of cell width r_0 inside the capillary. With a decrease in PO_2, RBCs become more deformable due to the deoxyHb–band 3 and band 3–cytoskeletal interactions and have a reduced cell width r_0.

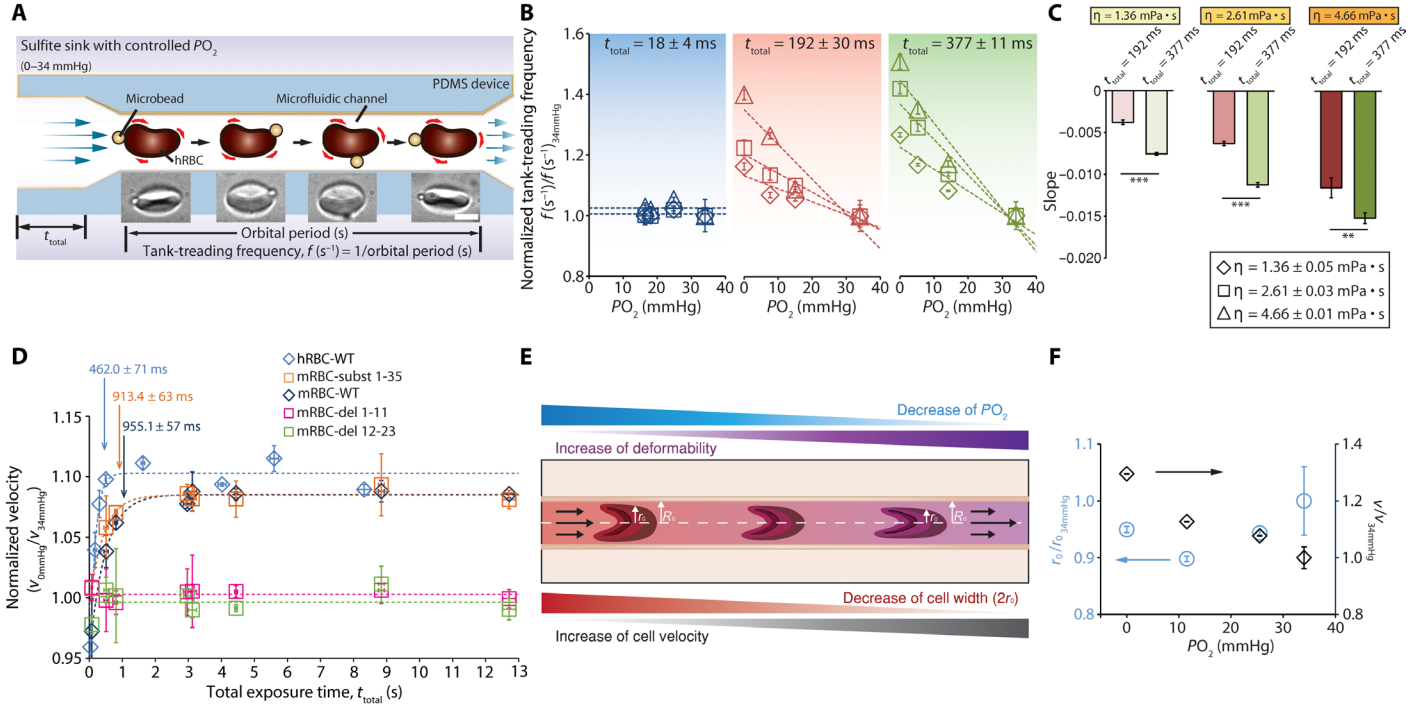

Fig. 4. Dynamics of PO_2-mediated RBC capillary velocity. (**A**) Schematics of experimental setup for ex vivo analysis of RBC tank-treading frequency, f (s^{-1}), at reduced PO_2. Human RBCs with microbeads (1 μm, polystyrene) attached on the cell membrane (inset images) were injected into a microfluidic channel with a constriction. f (s^{-1}) was calculated on the basis of the orbital periods (the time for the microbead moving along with the membrane for one revolution) of the microbead. t_{total} is the total exposure time of reduced PO_2 that RBC experienced before constriction and controlled by varying the length of the channel before constriction. Scale bar, 5 μm. (**B**) Normalized f (s^{-1}) as a function of PO_2 at different t_{total}. Dextran was added to increase the viscosity of RBC suspension. f (s^{-1}) was normalized by dividing f (s^{-1}) at PO_2 = 34 mmHg. f (s^{-1})/f (s^{-1})$_{34mmHg}$ did not change with PO_2 when t_{total} = 18 ± 4 ms but increased linearly with the decrease of PO_2 when t_{total} = 192 ± 30 and 377 ± 11 ms. The sensitivity to PO_2 changes increased as the increase of viscosity. At t_{total} = 192 ± 30 ms, η = 1.36 mPa·s: n = 80, f (s^{-1})/f (s^{-1})$_{34mmHg}$ = −0.0043 × PO_2 (mmHg) + 1.1326, R^2 = 0.839; η = 2.61 mPa·s: n = 116, f (s^{-1})/f (s^{-1})$_{34mmHg}$ = −0.0062 × PO_2 (mmHg) + 1.2036, R^2 = 0.959; η = 4.66 mPa·s: n = 120, f (s^{-1})/f (s^{-1})$_{34mmHg}$ = −0.0115 × PO_2 (mmHg) + 1.3509, R^2 = 0.874. At t_{total} = 377 ± 11 ms, η = 1.36 mPa·s: n = 129, f (s^{-1})/f (s^{-1})$_{34mmHg}$ = −0.0072 × PO_2 (mmHg) + 1.2253, R^2 = 0.894; η = 2.61 mPa·s: n = 160, f (s^{-1})/f (s^{-1})$_{34mmHg}$ = −0.0117 × PO_2 (mmHg) + 1.3677, R^2 = 0.920; η = 4.66 mPa·s: n = 120, f (s^{-1})/f (s^{-1})$_{34mmHg}$ = −0.0141 × PO_2 (mmHg) + 1.4461, R^2 = 0.924. (**C**) Effect of t_{total} on the sensitivity of f (s^{-1})/f (s^{-1})$_{34mmHg}$ to PO_2 changes. **P < 0.01 and ***P < 0.001, t test. (**D**) Normalized RBC capillary velocity V_{0mmHg}/V_{34mmHg} (where V_{0mmHg} and V_{34mmHg} are RBC velocity at PO_2 = 0 mmHg and PO_2 = 34 mmHg, respectively) as a function of t_{total}. Critical t_{total} beyond which RBC velocity did not change with t_{total} was identified as 462 ± 71, 913.4 ± 63, and 955.1 ± 57 ms for hRBC-WT, mRBC-subst 1-35, and mRBC-WT, respectively. (**E**) Schematics of the relation between PO_2, RBC deformability, and RBC capillary velocity. RBCs become more deformable at reduced PO_2 and thus have a smaller cell width (r_0) when flowing in a capillary with a diameter of $2R_0$. As a result, the gap distance between the surface of RBC and the capillary wall (R_0 − r_0) increases, leading to reduced hydrodynamic drag and thus increased RBC velocity. (**F**) Experimental measured changes of RBC width r_0 and RBC velocity v as a function of PO_2. $r_{0\ 34mmHg}$ and v_{34mmHg} were r_0 and v, respectively, at PO_2 = 34 mmHg. Error bars are shown as SE.

This decrease in r_0 leads to an increase in the gap distance between the channel wall and RBC membrane and reduces hydrodynamic drag, which in turn increases RBC capillary velocity.

DISCUSSION

Recent studies have revealed that functional hyperemia is initiated in capillaries (*14*, *15*) and that RBCs themselves can act as oxygen-sensing regulators to control capillary RBC velocity in response to local PO_2 changes (*15*). However, the underlying mechanisms of how PO_2 could modulate RBC velocity in capillaries are unknown. Experimental findings presented here implicate that deoxyHb–band 3 interactions in RBCs are the molecular switch that responds to local PO_2 changes and controls RBC deformability and consequently RBC capillary velocity. Evidently, we showed that (i) while ex vivo capillary velocity and deformation of mRBC-WT and mRBC-subst 1-35 exhibited a linear relation with local PO_2 changes, RBCs from transgenic mice that had enhanced or weakened deoxyHb–band 3 interactions showed capillary velocity and deformation independent of PO_2. RBCs with enhanced deoxyHb–band 3 interactions showed higher capillary velocity and deformability compared to RBCs that had weakened deoxyHb–band 3 interactions. (ii) Consistent with ex vivo results, in vivo cerebral capillary hyperemia in WT mice (mRBC-WT) and mRBC-subst 1-35 but not that with enhanced or weakened deoxyHb–band 3 interactions was dependent on local PO_2 changes. (iii) Direct dissociation of band 3–ankyrin interactions in both mRBC-WT and hRBCs via pervanadate treatment resulted in PO_2-independent RBC capillary velocity and deformation. Changing the amount of deoxyHb available to band 3 interactions by manipulating the intracellular concentration of 2,3-DPG via Pi or PEP treatment reduced the sensitivity of RBC capillary velocity, and deformation to PO_2 changes. RBCs with increased 2,3-DPG (via Pi treatment) showed higher capillary velocity and deformability compared to RBCs that had decreased 2,3-DPG (via PEP treatment). (iv) RBC membrane tank-treading frequency increased linearly with the decrease in PO_2. The magnitude and sensitivity of tank-treading frequency

to PO_2 changes increased with the increase in PO_2 exposure time and medium viscosity. (v) RBC capillary velocity depended on the duration of reduced PO_2 until a threshold exposure time, beyond which RBC velocity remained maximum and did not change with the exposure time anymore. Collectively, these sets of data indicate that RBC deoxyHb–band 3 and band 3–cytoskeletal interactions regulate PO_2-mediated RBC capillary velocity and that both the magnitude and duration of reduced PO_2 play critical roles.

The observation of the independence of RBC capillary velocity and deformation on PO_2 changes in mRBC-del 12-23 and RBCs treated with pervanadate has led us to conclude that RBCs could not either sense PO_2 changes when the deoxyHb binding site on band 3 was deleted or react to PO_2 changes when band 3–ankyrin interactions were disrupted. However, the reason why RBCs with enhanced deoxyHb–band 3 interactions (mRBC-del 1-11) did not respond to PO_2 changes is less obvious. Among other possible reasons, we speculate that the modified deoxyHb–band 3 binding kinetics in mRBC-del 1-11 and the relatively low PO_2 level in the present study play a role. It is known that the average copies of Hb and band 3 per RBC is approximately 270,000,000 and 1,200,000, respectively (*36*). As a result, less than 0.5% Hb is needed to bind band 3 during deoxygenation. Deoxygenation of such a small amount of Hb requires almost negligible decrease of PO_2 (*37*). Under the current experimental conditions where PO_2 = 34 mmHg, it is likely that all the Hb that is available to band 3 was already deoxygenated. Because the inhibitory residues 1 to 11 on band 3 were deleted in mRBC-del 1-11, deoxyHb–band 3 association in mRBC-del 1-11 was stronger and faster compared to that in WT RBCs (*27*). As a result, as soon as Hb is deoxygenated and available to band 3, it will bind band 3 readily. Therefore, further decrease of PO_2 from 34 to 0 mmHg will not affect the established deoxyHb–band 3 interactions and consequently cannot regulate RBC capillary velocity and deformation. The deoxyHb–band 3 interactions in WT RBCs are reversible, and the kinetic binding process depends on the concentration of available deoxyHb. As a result, the deformability and capillary velocity of WT RBCs are PO_2 dependent. Furthermore, despite the fact that the velocity and deformation index of mRBC-del 1-11 and mRBC-del 12-23 are PO_2 independent, the fact that mRBC-del 1-11 has a relatively high velocity and deformation index at PO_2 = 34 mmHg (Fig. 1, E and I) compared to that of mRBC-WT and mRBC-del 12-23 at the same PO_2 further confirms our hypothesis.

The effect of the duration of reduced PO_2 (t_{total}) on RBC capillary velocity, together with the critical t_{total} observed in Fig. 4D, highlights several important kinetic processes. First, there is a PO_2 equilibrium process when RBC suspension is injected into the microfluidic channel that has a reduced PO_2. The time scale of this process, t_{diff}, can be calculated on the basis of the dimensions of the channel before constriction (w = 50 μm; h = 4.5 μm) and the O_2 diffusion constant in water [$D_{diff} = 2.1 \times 10^{-9}$ m^2/s (*37*)], $t_{diff} = wh/4D_{diff}$, and is approximately 27 ms. This fast PO_2 equilibrium process is evidenced experimentally by the constant fluorescence intensity of an oxygen-sensitive dye flowing through the channel (fig. S4F). Second, after the PO_2 equilibrium is established between the channel and RBC suspension, RBCs will experience the reduced PO_2 in the medium and deoxygenation of RBCs occurs. For an RBC exposed to a zero PO_2 at the cell boundary, the approximate time to achieve 50% desaturation, t_{deoxy}, is about 30 to 50 ms (*38*, *39*), although a longer time of 100 to 150 ms has also been observed (*37*, *40*). In our case, the time required to deoxygenate 0.5% Hb necessary for band 3 interaction is expected to be much shorter than the reported t_{deoxy}. Third, during RBC deoxygenation, deoxyHb binds band 3, and band 3–ankyrin dissociation starts to occur. The kinetics of deoxyHb–band 3 binding is fast [the on-rate k_{on} and binding constant K_A are on the order of 10^6/M s (*41*) and 10^6/M (*26*, *42*), respectively], whereas the band 3–ankyrin dissociation is very slow [the off-rate k_{off} and dissociation constant K_d are on the order of 10^{-3}/s (*43*) and 10^{-8} M (*44*, *45*), respectively]. Thus, if the observed critical t_{total} represents these three kinetic processes, then band 3–ankyrin dissociation will be the rate-limiting step and likely accounts for the critical t_{total}. As a result, band 3–ankyrin dissociation may be more important to the physiologic process, while the deoxyHb–band 3 interactions serve to maintain that dissociated state. Meanwhile, note that although the kinetics of deoxyHb–band 3 interactions is fast, it may also affect the kinetics of PO_2-mediated RBC capillary velocity among different species. This is because the high-affinity ankyrin binding sites on band 3 are conserved among different species (*29*), but Hb–band 3 interactions are species specific and hRBCs have a higher binding affinity than mRBCs (*26*, *46*, *47*). Evidently, we observed in the present study that hRBCs have the shortest critical t_{total}, followed by mRBC-subst 1-35 and mRBC-WT. In addition, mRBC-subst 1-35 has the shorter in vivo onset time of capillary hyperemia than WT mouse. Regardless of different kinetic processes between species, the fact that the critical t_{total} from either hRBCs or mRBC-WT is shorter than the in vivo RBC capillary transit time (*48*–*50*) suggests that RBCs can adjust their properties to local PO_2 changes before exiting the capillary and thus facilitate O_2 delivery and extraction.

Last, RBC volume might change during RBC deoxygenation and may contribute to PO_2-mediated RBC capillary velocity. Several lines of evidence have suggested that deoxyHb–band 3 interactions trigger conformational changes of band 3 (*51*) and regulate RBC ion flux including RBC volume regulatory transporters (*52*–*54*). In addition, Piezo1, the mechanosensing ion channel on RBCs, is likely to be activated during capillary transit (*55*) and controls RBC volume (*56*). Whether and how RBC volume contributes PO_2-mediated RBC capillary velocity are of interest for further studies, the present results nevertheless demonstrate that deoxyHb–band 3 and band 3–ankyrin interactions play critical roles in PO_2-mediated RBC capillary velocity and contribute to cerebral functional hyperemia. These findings not only advance our understanding of the mechanisms of functional hyperemia in the brain but also provide universal principles of RBC-based blood flow regulation, and thus open up new opportunities to study neurodegenerative disease such as vascular dementia, where RBCs may contribute to the dysfunctions of blood flow regulation and, consequently, the observed neurodegenerative conditions.

MATERIALS AND METHODS

Animals and surgical preparation

Three strains of transgenic mice (mRBC-subst 1-35, mRBC-del 1-11, and mRBC-del 12-23) were provided by D. Bodine from the National Institutes of Health. WT mice (mRBC-WT, C57BL/6J) were purchased from the Jackson Laboratory. Anesthesia was induced in experimental animals with 2.0% isoflurane in oxygen and maintained at 1.5 to 2.0% during surgical preparation. The depth of anesthesia was monitored by toe pinch and whisker movement. Body temperature was maintained by a water-perfused thermal pad (Gaymar T/Pump) set at 37°C. A custom-made metal plate was glued

to the skull, and a 1.5- to 2.5-mm-diameter cranial window was made over the hindlimb cortex for imaging (stereotaxic coordinates, 0.5 to 3 mm lateral and −1.5 to +1 mm anterior of bregma). Agarose (1.1% in artificial cerebrospinal fluid at 37°C) was applied, and a glass coverslip was sealed to the metal plate. All experimental procedures were approved by the University Committee on Animal Resources at the University of Rochester, and effort was taken to minimize the number of animals used. This research was approved by the institutional review boards at the Rochester Institute of Technology and the University of Rochester School of Medicine.

RBC preparation and treatment

Whole blood was extracted from mice or healthy human donors and prepared on the day of use. RBCs were separated from plasma by centrifuging 1 ml of whole blood at 300*g* at 20°C for 1.5 min. The supernatant was removed by aspiration. The packed RBCs were resuspended and washed three times in PBS buffer. The RBCs were then diluted with a PBS solution (3%, v/v). Note that for all mRBCs, PBS buffer was prepared as follows: 152 mM NaCl, 2.7 mM KCl, 8.1 mM Na_2HPO_4, 1.47 KH_2PO_4, and 10 mM glucose (pH 7.4) (osmolality, 340 mOsm/kg). For hRBCs, PBS buffer was used as purchased from Thermo Fisher Scientific (pH 7.2) (osmolality, 280 to 320 mOsm/kg; catalog no. 20012027). PEP (phosphoenolpyruvate) and P_i (sodium phosphate) solutions were prepared in PBS as follows: 50 mM PEP, 28.8 mM Mannitol, 50 mM glucose, 20 mM NaCl, and 1 mM adenine for PEP solution; and 50 mM P_i, 28.8 mM Mannitol, 50 mM glucose, 20 mM NaCl, and 1 mM adenine for P_i solution. pH of the solutions was adjusted to 6.0. Packed RBCs were suspended in either PEP or P_i solution, incubated for 1 hour at 37°C, and then washed twice with PBS. To determine the concentration of 2,3-DPG in RBCs, ultraviolet testing was conducted following the manufacturing protocol of Sigma Kit (catalog no. 10148334001, Sigma-Aldrich). In pervanadate treatment, packed RBCs were suspended in PBS with 0.5 mM sodium orthovanadate and 150 mM H_2O_2. After incubation at 37°C for 30 min, RBCs were washed three times using PBS and resuspended in a fresh PBS with glucose for 180 min to obtain 100% phosphorylation of band 3 and ankyrin.

Microfluidic device and RBC imaging

Microfluidic devices were fabricated with PDMS using standard soft photolithography techniques. The microfluidic device was connected via a short polyethylene (PE 20) tube to an RBC reservoir where a constant pressure (1.1×10^4 Pa) was applied using a gas regulator (DPG1001B, OMEGA) with a precision of 689 Pa. To control PO_2 inside the channel, the entire microfluidic device was immersed in a customized glass chamber filled with an aqueous solution containing 0, 0.01, 0.1, or 1.0 M sodium sulfite (Sigma-Aldrich), and the PO_2 inside was equilibrated with the surrounding environment for 20 min before experiments. Although in vivo PO_2 in capillaries varies in a wide range (i.e., ~5 to 95 mmHg), it tends to stay at the lower end of that range for most cases. Thus, a PO_2 between 0 to 34 mmHg was chosen for the ex vivo microfluidic studies. For each experiment, RBCs from at least three mice or human individuals were used, and one to two microfluidic devices per mouse or human sample were used.

PO_2 calibration in microfluidics

To colorimetrically quantify the PO_2 in the microfluidic channel, 25 μM tris(2,2′-bipyridyl)dichlororuthenium(II) hexahydrate (an O_2 indicator; Sigma-Aldrich) was prepared in N_2-bubbled or air-saturated deionized water and injected into the microfluidic device at a constant pressure (1.1×10^4 Pa). The change in fluorescence intensity of the O_2 indicator flowing through the microfluidic device was measured using a RatioMaster system (Photon Technology International) and converted to a PO_2 value using the Stern-Volmer equation, $I_0/I = 1 + PO_2 \times K_q$, in which I_0 is the maximum of the fluorescence intensity and K_q is the quenching constant. To calculate I_0 and K_q, we used PO_2 of 34 and 174 mmHg, respectively, in N_2-bubbled dye solution (after bubbling for 16 hours) and air-saturated dye solution, which was measured and calibrated using a World Precision Instruments dissolved O_2 meter and a Bayer Rapidlab 248 blood gas analyzer. These values of I_0 and K_q were then used to calculate PO_2 in microfluidic channels.

RBC velocity and deformability measurement

To measure mRBC velocity, we injected mRBCs into a microfluidic device with a constriction of w_c = 3 μm and h = 4.5 μm at a constant pressure of 1.1×10^4 Pa. The movements of mRBCs in the constriction were recorded using a high-speed video camera (Phantom Miro M120; 1900 frames/s) mounted on an inverted microscope (Leica DMI6000B). The recorded videos were analyzed using Phantom Camera Control software and ImageJ, and mRBC velocity was calculated assuming a steady flow condition. To determine the deformability of mRBCs, we used a microfluidic device with a constriction of w_c = 10 μm and h = 7.4 μm. The deformation of mRBCs flowing through the constriction was recorded using the high-speed camera and characterized by the change of elongation index D_l/D_w, where D_l and D_w are the length and thickness of mRBC, respectively. To examine human RBC velocity and deformation as a function of PO_2, we used the same approach as described above expect that a microfluidic device with a constriction of w_c = 5 μm and h = 7 μm and w_c = 20 μm and h = 30 μm was used, respectively, for the hRBC velocity and deformation measurement. To study the effect of total exposure time of reduced PO_2 on RBC velocity, we used microfluidic devices with different lengths of channel before the constriction (100, 500, 1000, 1500, 3000, 5000, 7000, and 9000 μm) to control the total exposure time. In this case, the PO_2 was controlled at 0 and 34 mmHg.

RBC tank-treading frequency measurement

A microfluidic channel containing a constriction (w_c = 20 μm; h = 38 μm) was used to measure tank-treading frequency of hRBCs. The microfluidic device was immersed in a sulfite sink with different concentrations of sodium sulfite (0, 0.01, 0.1, and 1 M). The length of the channel before constriction was varied from 600, 4200, and 12000 μm to obtain a total exposure time of 18 ± 4, 192 ± 30, and 377 ± 11 ms, respectively. hRBC suspension (1 ml) in PBS (1.5%, v/v) was mixed with 10 μl of polystyrene microspheres [0.5% (w/v) in PBS; Polybead, Polysciences Inc.] and injected into the microfluidic channel. Dextran (*Leuconostoc* spp., relative molecular mass of 450,000 to 650,000; Sigma-Aldrich) was added to increase the viscosity of RBC suspension from 1.36 and 2.61 mPa·s to 4.66 mPa·s, as measured using a rheometer (Discovery HR-2 Hybrid Rheometer, TA Instruments). The rotation of the microbead on RBCs was recorded using a high-speed camera, and the tank-treading frequency was calculated as 1/the time for the microbead moving along with the membrane for one revolution. Note that to maintain a relatively constant velocity when the viscosity of RBC suspension was changed, the inject pressure was changed from 3.45×10^3 to 8.96×10^3, accordingly.

In vivo two-photon imaging

Two-photon imaging was performed using a Thorlabs two-photon setup attached to a Mai Tai HP Ti:Sapphire laser (Spectra-Physics). A 20× objective (0.9 numerical apperture; Olympus) was used. Intravascular fluorescein isothiocyanate–dextran (FITC-dextran; 2.5% in saline) was injected to the tail of the mouse and excited at 820 nm. To prepare the sulfite puffing solution, 0.01 or 1 M sodium sulfite was dissolved in 10 mM Hepes (with a drop of HCl to adjust pH to 7.3) containing 100 μM Alexa Fluor 594 and loaded into a glass micropipette with a tip diameter of 2 to 3 μm. The puffing micropipette was then carefully loaded into a capillary bed in the cerebral cortex, and the sulfite solution was puffed at 10 psi (~20 ms) controlled by a Picospritzer III. Capillary RBC velocity was captured with line scans (scan rate, ~1 kHz) placed along the length of the capillary. RBC velocities ($\Delta x/\Delta t$, mm/s) were calculated from parallel-to-flow line-scan images using the contrast between FITC-dextran–labeled plasma and unlabeled RBCs, using a modified version of the LS-PIV algorithm in MATLAB.

Local tissue PO_2 measurement

Local tissue O_2 tension was recorded with a calibrated modified Clark-type polarographic O_2 microelectrode (OX-10, Unisense A/S, Aarhus, Denmark) inserted in close proximity to the puffing pipette (~50 μm). The signal was amplified and analog-to-digital converted by a high-impedance picoammeter (OXY-Meter, Unisense A/S). Data were recorded in pCLAMP 9.0 and analyzed using Clampfit 10.4 and MATLAB.

Parameter estimation

A zero-phase running average filter (window size, ~1 s) was used to smooth raw velocity data after outliers (raw data points of >3 SDs from mean of trace) were removed. Onset of the evoked response was estimated by fitting a line to the slope between 20 and 80% to the peak of the response and calculating the time of the line's x intercept. Five to 10 s immediately before puffing stimulation was considered baseline, and responses occurring within 20 s after the start of stimulation were analyzed.

SUPPLEMENTARY MATERIALS

Supplementary material for this article is available at http://advances.sciencemag.org/cgi/content/full/5/5/eaaw4466/DC1

Fig. S1. Calibration of oxygen level in microfluidic channels.

Fig. S2. Baseline RBC velocity in WT mice and transgenic mice before sulfite puffing.

Fig. S3. RBC 2,3-DPG and capillary velocity changes upon PEP and Pi treatments.

Fig. S4. Effect of medium viscosity on PO_2-regulated RBC tank-treading frequency and the calculation of RBC capillary velocity as a function of RBC size.

REFERENCES AND NOTES

1. C. Iadecola, Neurovascular regulation in the normal brain and in Alzheimer's disease. *Nat. Rev. Neurosci.* **5**, 347–360 (2004).
2. C. Iadecola, The neurovascular unit coming of age: A journey through neurovascular coupling in health and disease. *Neuron* **96**, 17–42 (2017).
3. M. E. Raichle, Behind the scenes of functional brain imaging: A historical and physiological perspective. *Proc. Natl. Acad. Sci. U.S.A.* **95**, 765–772 (1998).
4. I. Vanzetta, A. Grinvald, Increased cortical oxidative metabolism due to sensory stimulation: Implications for functional brain imaging. *Science* **286**, 1555–1558 (1999).
5. P. B. Gorelick, S. E. Counts, D. Nyenhuis, Vascular cognitive impairment and dementia. *Biochim. Biophys. Acta* **1862**, 860–868 (2016).
6. A. Khan, R. N. Kalaria, A. Corbett, C. Ballard, Update on vascular dementia. *J. Geriatr. Psychiatry Neurol.* **29**, 281–301 (2016).
7. K. Kisler, A. R. Nelson, A. Montagne, B. V. Zlokovic, Cerebral blood flow regulation and neurovascular dysfunction in Alzheimer disease. *Nat. Rev. Neurosci.* **18**, 419–434 (2017).
8. B. V. Zlokovic, Neurovascular pathways to neurodegeneration in Alzheimer's disease and other disorders. *Nat. Rev. Neurosci.* **12**, 723–738 (2011).
9. T. Hayashi, H. Watabe, N. Kudomi, K. M. Kim, J.-I. Enmi, K. Hayashida, H. Iida, A theoretical model of oxygen delivery and metabolism for physiologic interpretation of quantitative cerebral blood flow and metabolic rate of oxygen. *J. Cereb. Blood Flow Metab.* **23**, 1314–1323 (2003).
10. M. A. Mintun, B. N. Lundstrom, A. Z. Snyder, A. G. Vlassenko, G. L. Shulman, M. E. Raichle, Blood flow and oxygen delivery to human brain during functional activity: Theoretical modeling and experimental data. *Proc. Natl. Acad. Sci. U.S.A.* **98**, 6859–6864 (2001).
11. R. B. Buxton, L. R. Frank, A model for the coupling between cerebral blood flow and oxygen metabolism during neural stimulation. *J. Cereb. Blood Flow Metab.* **17**, 64–72 (2016).
12. D. R. Harder, N. J. Alkayed, A. R. Lange, D. Gebremedhin, R. J. Roman, Functional hyperemia in the brain: Hypothesis for astrocyte-derived vasodilator metabolites. *Stroke* **29**, 229–234 (1998).
13. A. R. Nippert, K. R. Biesecker, E. A. Newman, Mechanisms mediating functional hyperemia in the brain. *Neuroscientist* **24**, 73–83 (2017).
14. C. N. Hall, C. Reynell, B. Gesslein, N. B. Hamilton, A. Mishra, B. A. Sutherland, F. M. O'Farrell, A. M. Buchan, M. Lauritzen, D. Attwell, Capillary pericytes regulate cerebral blood flow in health and disease. *Nature* **508**, 55–60 (2014).
15. H. S. Wei, H. Kang, I.-Y. D. Rasheed, S. Zhou, N. Lou, A. Gershteyn, E. D. McConnell, Y. Wang, K. E. Richardson, A. F. Palmer, C. Xu, J. Wan, M. Nedergaard, Erythrocytes are oxygen-sensing regulators of the cerebral microcirculation. *Neuron* **91**, 851–862 (2016).
16. R. A. Hill, L. Tong, P. Yuan, S. Murikinati, S. Gupta, J. Grutzendler, Regional blood flow in the normal and ischemic brain is controlled by arteriolar smooth muscle cell contractility and not by capillary pericytes. *Neuron* **87**, 95–110 (2015).
17. F. Fernández-Klett, N. Offenhauser, U. Dirnagl, J. Priller, U. Lindauer, Pericytes in capillaries are contractile in vivo, but arterioles mediate functional hyperemia in the mouse brain. *Proc. Natl. Acad. Sci. U.S.A.* **107**, 22290–22295 (2010).
18. K. Kisler, A. R. Nelson, S. V. Rege, A. Ramanathan, Y. Wang, A. Ahuja, D. Lazic, P. S. Tsai, Z. Zhao, Y. Zhou, D. A. Boas, S. Sakadžić, B. V. Zlokovic, Pericyte degeneration leads to neurovascular uncoupling and limits oxygen supply to brain. *Nat. Neurosci.* **20**, 406–416 (2017).
19. M. D. Sweeney, S. Ayyadurai, B. V. Zlokovic, Pericytes of the neurovascular unit: Key functions and signaling pathways. *Nat. Neurosci.* **19**, 771–783 (2016).
20. I. Messana, M. Orlando, L. Cassiano, L. Pennacchietti, C. Zuppi, M. Castagnola, B. Giardina, Human erythrocyte metabolism is modulated by the O_2-linked transition of hemoglobin. *FEBS Lett.* **390**, 25–28 (1996).
21. I. A. Lewis, M. E. Campanella, J. L. Markley, P. S. Low, Role of band 3 in regulating metabolic flux of red blood cells. *Proc. Natl. Acad. Sci. U.S.A.* **106**, 18515–18520 (2009).
22. N. N. Barvitenko, N. C. Adragna, R. E. Weber, Erythrocyte signal transduction pathways, their oxygenation dependence and functional significance. *Cell. Physiol. Biochem.* **15**, 1–18 (2015).
23. G. R. Bergfeld, T. Forrester, Release of ATP from human erythrocytes in response to a brief period of hypoxia and hypercapnia. *Cardiovasc. Res.* **26**, 40–47 (1992).
24. H. Chu, M. M. McKenna, N. A. Krump, S. Zheng, L. Mendelsohn, S. L. Thein, L. J. Garrett, D. M. Bodine, P. S. Low, Reversible binding of hemoglobin to band 3 constitutes the molecular switch that mediates O_2 regulation of erythrocyte properties. *Blood* **128**, 2708–2716 (2016).
25. M. Stefanovic, E. Puchulu-Campanella, G. Kodippili, P. S. Low, Oxygen regulates the band 3-ankyrin bridge in the human erythrocyte membrane. *Biochem. J.* **449**, 143–150 (2013).
26. M. F. Sega, H. Chu, J. A. Christian, P. S. Low, Fluorescence assay of the interaction between hemoglobin and the cytoplasmic domain of erythrocyte membrane band 3. *Blood Cells Mol. Dis.* **55**, 266–271 (2015).
27. H. Chu, A. Breite, P. Ciraolo, R. S. Franco, P. S. Low, Characterization of the deoxyhemoglobin binding site on human erythrocyte band 3: Implications for O_2 regulation of erythrocyte properties. *Blood* **111**, 932–938 (2008).
28. M. F. Sega, H. Chu, J. Christian, P. S. Low, Interaction of deoxyhemoglobin with the cytoplasmic domain of murine erythrocyte band 3. *Biochemistry* **51**, 3264–3272 (2012).
29. D. Zhang, A. Kiyatkin, J. T. Bolin, P. S. Low, Crystallographic structure and functional interpretation of the cytoplasmic domain of erythrocyte membrane band 3. *Blood* **96**, 2925–2933 (2000).
30. J. A. Walder, R. Chatterjee, T. L. Steck, P. S. Low, G. F. Musso, E. T. Kaiser, P. H. Rogers, A. Arnone, The interaction of hemoglobin with the cytoplasmic domain of band 3 of the human erythrocyte membrane. *J. Biol. Chem.* **259**, 10238–10246 (1984).
31. L. Bordin, F. Ion-Popa, A. M. Brunati, G. Clari, P. S. Low, Effector-induced Syk-mediated phosphorylation in human erythrocytes. *Biochim. Biophys. Acta* **1745**, 20–28 (2005).
32. E. Ferru, K. Giger, A. Pantaleo, E. Campanella, J. Grey, K. Ritchie, R. Vono, F. Turrini, P. S. Low, Regulation of membrane-cytoskeletal interactions by tyrosine phosphorylation of erythrocyte band 3. *Blood* **117**, 5998–6006 (2011).
33. H. Kimura, N. Hamasaki, M. Yamamoto, M. Tomonaga, Circulation of red blood cells having high levels of 2,3-bisphosphoglycerate protects rat brain from ischemic metabolic changes during hemodilution. *Stroke* **26**, 1431–1437 (1995).
34. A. Arnone, X-ray diffraction study of binding of 2,3-diphosphoglycerate to human deoxyhaemoglobin. *Nature* **237**, 146–149 (1972).

35. A. M. Forsyth, J. Wan, P. D. Owrutsky, M. Abkarian, H. A. Stone, Multiscale approach to link red blood cell dynamics, shear viscosity, and ATP release. *Proc. Natl. Acad. Sci. U.S.A.* **108**, 10986–10991 (2011).
36. P. S. Low, Structure and function of the cytoplasmic domain of band 3: Center of erythrocyte membrane-peripheral protein interactions. *Biochim. Biophys. Acta* **864**, 145–167 (1986).
37. K. D. Vandegriff, J. S. Olson, The kinetics of O_2 release by human red blood cells in the presence of external sodium dithionite. *J. Biol. Chem.* **259**, 12609–12618 (1984).
38. A. S. Popel, Theory of oxygen transport to tissue. *Crit. Rev. Biomed. Eng.* **17**, 257–321 (1989).
39. R. A. Holland, H. Shibata, P. Scheid, J. Piiper, Kinetics of O_2 uptake and release by red cells in stopped-flow apparatus: Effects of unstirred layer. *Respir. Physiol.* **59**, 71–91 (1985).
40. J. T. Coin, J. S. Olson, The rate of oxygen uptake by human red blood cells. *J. Biol. Chem.* **254**, 1178–1190 (1979).
41. N. Shaklai, V. S. Sharma, Kinetic study of the interaction of oxy- and deoxyhemoglobins with the erythrocyte membrane. *Proc. Natl. Acad. Sci. U.S.A.* **77**, 7147–7151 (1980).
42. R. Cassoly, Quantitative analysis of the association of human hemoglobin with the cytoplasmic fragment of band 3 protein. *J. Biol. Chem.* **258**, 3859–3864 (1983).
43. W. A. Anong, T. L. Weis, P. S. Low, Rate of rupture and reattachment of the band 3-ankyrin bridge on the human erythrocyte membrane. *J. Biol. Chem.* **281**, 22360–22366 (2006).
44. B. J. Thevenin, P. S. Low, Kinetics and regulation of the ankyrin-band 3 interaction of the human red blood cell membrane. *J. Biol. Chem.* **265**, 16166–16172 (1990).
45. H. M. Van Dort, R. Moriyama, P. S. Low, Effect of band 3 subunit equilibrium on the kinetics and affinity of ankyrin binding to erythrocyte membrane vesicles. *J. Biol. Chem.* **273**, 14819–14826 (1998).
46. R. R. Kopito, H. F. Lodish, Structure of the murine anion exchange protein. *J. Cell. Biochem.* **29**, 1–17 (1985).
47. Q. Chen, T. C. Balazs, R. L. Nagel, R. E. Hirsch, Human and mouse hemoglobin association with the transgenic mouse erythrocyte membrane. *FEBS Lett.* **580**, 4485–4490 (2006).
48. S. N. Jespersen, L. Ostergaard, The roles of cerebral blood flow, capillary transit time heterogeneity, and oxygen tension in brain oxygenation and metabolism. *J. Cereb. Blood Flow Metab.* **32**, 264–277 (2011).
49. R. G. Presson Jr., J. A. Graham, C. C. Hanger, P. S. Godbey, S. A. Gebb, R. A. Sidner, R. W. Glenny, W. W. Wagner Jr., Distribution of pulmonary capillary red blood cell transit times. *J. Appl. Physiol.* **79**, 382–388 (1985).
50. G. S. Zavorsky, K. R. Walley, J. A. Russell, Red cell pulmonary transit times through the healthy human lung. *Exp. Physiol.* **88**, 191–200 (2003).
51. J. M. Salhany, R. Cassoly, Kinetics of *p*-mercuribenzoate binding to sulfhydryl groups on the isolated cytoplasmic fragment of band 3 protein. Effect of hemoglobin binding on the conformation. *J. Biol. Chem.* **264**, 1399–1404 (1989).
52. J. S. Gibson, P. F. Speake, J. C. Ellory, Differential oxygen sensitivity of the K^+-Cl^- cotransporter in normal and sickle human red blood cells. *J. Physiol.* **511**, 225–234 (1998).
53. M. C. Muzyamba, E. H. Campbell, J. S. Gibson, Effect of intracellular magnesium and oxygen tension on K^+-Cl^- cotransport in normal and sickle human red cells. *Cell. Physiol. Biochem.* **17**, 121–128 (2006).
54. C. Drew, V. Ball, H. Robinson, J. Clive Ellory, J. S. Gibson, Oxygen sensitivity of red cell membrane transporters revisited. *Bioelectrochemistry* **62**, 153–158 (2004).
55. E. Cinar, S. Zhou, J. DeCourcey, Y. Wang, R. E. Waugh, J. Wan, Piezo1 regulates mechanotransductive release of ATP from human RBCs. *Proc. Natl. Acad. Sci. U.S.A.* **112**, 11783–11788 (2015).
56. S. M. Cahalan, V. Lukacs, S. S. Ranade, S. Chien, M. Bandell, A. Patapoutian, Piezo1 links mechanical forces to red blood cell volume. *eLife* **4**, e07370 (2015).

Acknowledgments: We thank W. Song for helping with animal surgery and T. Allston for helping with the measurement of RBC 2,3-DPG concentration. We also thank D. Xue for helping with schematic illustrations and Y. Mori for checking the validity of the calculation of RBC velocity as a function of r_0. **Funding:** This work was supported by NIH grants 1RF1 NS110049-01 (to M.N. and J.W.) and R01 GM24417-39 (to P.S.L.). **Author contributions:** J.W., S.T.Z., and P.S.L. designed the research. J.W., S.T.Z., H.S.W., P.S.L., and M.N. wrote the manuscript. S.T.Z., M.G., and J.D. did the ex vivo microfluidic experiments. N.K., H.K., and J.W. did the in vivo two-photon experiments. Y.L., H.Z., and J.W. did the data analysis and calculation. S.L.Z., W.R.S., D.M.B., and P.S.L. worked on the transgenic mice. **Competing interests:** The authors declare that they have no competing interests. **Data and materials availability:** All data needed to evaluate the conclusions in the paper are present in the paper and/or the Supplementary Materials. Additional data related to this paper may be requested from the authors.

Submitted 20 December 2018
Accepted 17 April 2019
Published 29 May 2019
10.1126/sciadv.aaw4466

Citation: S. Zhou, M. Giannetto, J. DeCourcey, H. Kang, N. Kang, Y. Li, S. Zheng, H. Zhao, W. R. Simmons, H. S. Wei, D. M. Bodine, P. S. Low, M. Nedergaard, J. Wan, Oxygen tension–mediated erythrocyte membrane interactions regulate cerebral capillary hyperemia. *Sci. Adv.* **5**, eaaw4466 (2019).